XAFS studies of nickel-doped lead telluride

Ivana Radisavljević [a,*], Nikola Novaković [a], Nenad Ivanović [a], Nebojša Romčević [b], Miodrag Manasijević [a], Heinz-Eberhard Mahnke [c]

[a] Vinča Institute of Nuclear Sciences, University of Belgrade, POB 522, 11001 Belgrade, Serbia
[b] Institute of Physics, University of Belgrade, Pregrevica 118, 11000 Belgrade, Serbia
[c] Helmholtz-Zentrum Berlin für Materialien und Energie GmbH, D-14109 Berlin, Germany

ARTICLE INFO

ABSTRACT

The problem of impurities and defect states in lead telluride-based semiconductors is of crucial importance for their practical applications. X-ray absorption fine structure (XAFS) techniques are capable to address some of the key issues regarding impurities position, their valent state, as well as the local structural changes of the host lattice in the immediate surrounding of the impurity atoms. In this paper we present the results of the Ni K-absorption edge XAFS studies of Ni-doped PbTe at different temperatures. Analysis of near edge and extended XAFS regions of the measured spectra provided information about exact local environment and lattice ordering around Ni atoms.

1. Introduction

Lead telluride-based semiconductors are extensively used in optoelectronics and thermoelectronics [1–4], and recently also in spintronics and quantum electronics [5,6]. Such a wide range of their application is made possible by their unique properties (tunable direct energy gap, high efficiency of radiative recombination, high values of static dielectric constant, small effective mass of carriers, etc.) and versatile possibilities of their combination. Introduction of a particular dopant atom into the host material can lead to appearance of qualitatively new material properties. Whereas group III impurities induce interesting electronic (pinning of the free carriers concentration and Fermi level) and optical properties (strong plasmon–phonon coupling, activation of local optical modes), transition metals act as magnetic impurities and can provoke interesting effects such as giant magnetoresistance. In the case of a large difference between ionic radii and polarizability of the interchanging ions, impurity atoms are readily displaced from the regular lattice positions, creating that way dipoles whose ordering can lead to ferroelectric phase transitions [7,8]. Although a lot of work has been devoted to study defect states in lead telluride-based semiconductors [7–14] they are not yet fully understood. Most theoretical studies [12,13] assume impurities positioned at ideal lattice sites, which often proved not to be the case. Therefore, it is very important to resolve local structures around impurities in order to better understand their influence on macroscopic characteristics of the materials they are incorporated in.

Element specific X-ray absorption fine structure (XAFS) spectroscopy is at present one of the most powerful tools used for studying structural, electronic and magnetic properties of materials. The near edge region of the absorption spectrum (XANES) is sensitive on electronic structure and contains information on oxidation state and the local coordination geometry around the absorbing atom, whereas the high energy region (EXAFS) is associated with the arrangement of atoms and provides information about the short range order in terms of number, type and distances of atoms in coordination shells and their disorder parameters. Using XAFS spectroscopy we have already resolved the local structures in the series of lead telluride-based semiconductors [15–17]. In this work we extend our studies to Ni-doped PbTe, a semimagnetic semiconductor whose electronic and magnetic properties are not completely understood. Lead telluride crystallizes in rocksalt (NaCl)-type face-centered-cubic (FCC) structure (space group Fm3m, $a = 6.46$ Å), where both Pb and Te atoms are octahedrally coordinated with atoms of different kind. Nickel forms two types of tellurides: (i) antiferromagnetic semiconductor NiTe with a nickel arsenide (NiAs)-type crystal structure (space group P6$_3$/mmc, $a = 3.390$ Å, $c = 5.344$ Å [18]), where Ni occupy a simple cubic lattice which penetrates a close-packed hexagonal Te lattice, and (ii) paramagnetic metallic NiTe$_2$ with a cadmium iodide (CdI$_2$)-type crystal structure (space group P-3m1, $a = 3.861$, $c = 5.297$ Å [19]), where Te form a hexagonal close packed arrangement while Ni occupy all octahedral sites in alternate layers. Octahedral Te coordination of Ni atoms in both of these tellurides is what provides their partial solubility in PbTe.

* Corresponding author. Tel.: +381 11 3408610; fax: +381 11 3440100.
E-mail address: iva@vinca.rs (I. Radisavljević).

2. Experiment

XAFS measurements on PbTe:Ni ($n_{Ni} = 1 \times 10^{19}$ at/cm^3) single crystal [20] were performed at A1 beamline of HASYLAB at DESY. The synchrotron radiation source was operating at electron beam energy of 4.5 GeV with a maximum current of 200 mA. Samples were oriented at 45° to the incident beam and a 7-segment Ge-detector was used to collect spectra in fluorescence mode. XANES spectra were modelled with the real space multiple scattering code FEFF8.2 [21] using the self-consistent field approach with Hedin–Lundqvist exchange-correlation. Different atomic arrangements generated by ATOMS package [22] were used as FEFF input files. ATHENA and ARTEMIS packages [23,24] were used to analyze EXAFS data. Fourier transforms (FT) of the k-weighted EXAFS function $k\chi(k)$ were performed over the k range from 3 to 13 Å^{-1} using the Hanning windows. The k_{min} and k_{max} values were chosen at $\chi(k)$ node points to minimize the spectral broadening, while unphysical peaks in the low k-region are suppressed by taking $R_{bkg} = 1.5$. Number of atoms in the jth shell (N_j), mean distance of the jt shell (R_j), and mean-squared displacement of atoms in the jth shell (σ^2) were adjusted for each path during the fitting procedure. The same edge shift correction (ΔE_0) was used for all paths, and amplitude reduction factor (S_0^2) was set to 0.7. Fit-quality factor R, estimated by the reduced chi-square (χ_v^2) method as implemented in ARTEMIS, was less than 4%.

3. Results and discussion

3.1. XANES results

The K-edge XANES spectrum is determined by dipole 1s to 4p transitions, and the rising edge energy position is an approximate measure of the oxidation state of the absorbing atom. Transitions to d-states are formally forbidden but they can occur if there is mixing between 3d and 4p states, in which case they yield structure in the pre-edge region. Appearance of the pre-edge structure is rather common in the transition-metals absorption spectra, though its interpretation is still controversial. It is however known that higher symmetry of the metal site generally leads to weaker pre-edge structure. For the lattice sites with inversion symmetry orbital p–d mixing is not allowed, and pre-edge features are ascribed to quadrupole s–d transitions.

Fig. 1 shows experimental Ni K-edge XANES spectra recorded at three different temperatures (curves 6–8) and model spectra (curves 1–5) used in their analysis. Experimental spectra are almost identical, which means that the change of Ni immediate surrounding with temperature is insignificant. The similar edge position ($E_0 \approx 8338$ eV) in all experimental spectra implies that there is no major change of Ni valent state with rising temperature. The basic XANES model (curve 1) assumes Ni atom replacing Pb at the ideal PbTe lattice position. It turned out that there is a large mismatch between experimental and this model spectrum, whose main features remained almost unaffected after allowing the possibility of Ni atom displacement and also after Te vacancy introduction. The same is true for the model with Ni atoms in NiTe-like immediate surrounding (curve 2). The NiTe$_2$ model (curve 3) brought considerable improvement, although the shape of the main edge is still markedly different from the experimentally observed. The main edge shape slightly changes in the model that combines models 1 and 3 in the ratio 4:2 (curve 4), although it shows tendency to increase in intensity with increasing NiTe$_2$ content. The best description of the main edge part is achieved when Te octahedron is rotated from the NiTe$_2$-position so to match the orientation that it has in PbTe (curve 5). However, the high energy part of the model spectrum (which is
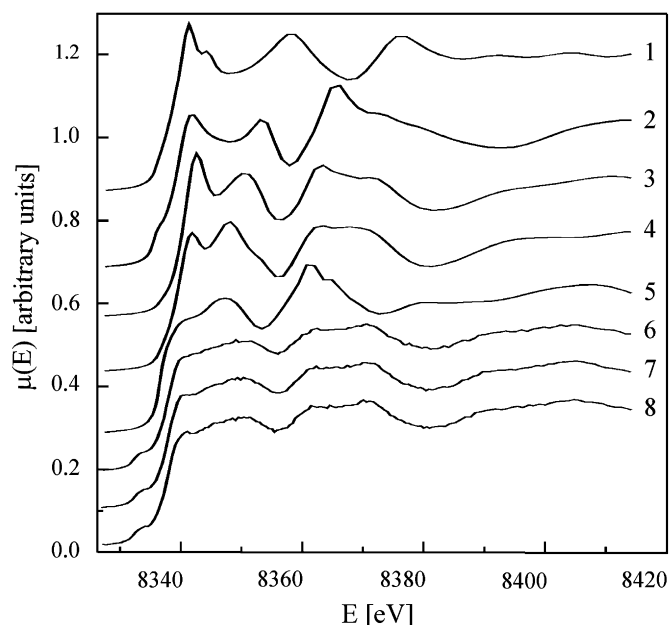

Fig. 1. Ni K-edge experimental XANES spectra (6–8) taken at 20, 80 K and RT, respectively, and theoretical models: 1—Ni replacing Pb at the ideal PbTe lattice position, 2—Ni as in NiTe, 3—Ni as in NiTe$_2$, 4—combination of models 1 and 3 in the ratio 4:2, and 5—Te octahedron surrounding Ni rotated from NiTe$_2$ to PbTe position.

influenced by multiple scattering processes and is therefore very difficult to interpret) is now completely different.

These results indicated very complicated structure of the Ni immediate surrounding which none of the employed models succeeded to reproduce. The origin of the pre-edge shoulder-like feature is also unclear. The symmetry of Ni sites could be violated due to the Te octahedron deformation, Ni atoms displacement or presence of Te vacancies. Even if the octahedral symmetry is preserved, the pre-edge structure could appear as a result of quadrupole s–d transitions. The lack of pre-edge structure in the model XANES spectra could be ascribed to limitations of the FEFF based calculations in reproducing near edge region, even though the possibility of quadrupole transition was included. The lack of appropriate reference sample hindered the determination of eventual presence of Ni atoms in valent states different than expected 2+.

3.2. EXAFS results

Analyses of the EXAFS results confirmed that the local structure around Ni atoms is completely different from that expected for PbTe and also for NiTe compound. In accordance with XANES analyses, the best fits of the experimental EXAFS spectra are obtained using the NiTe$_2$-structure model. These fits are presented in Fig. 2 and the parameters values are given in Table 1. Tellurium atoms in the first coordination shell are placed at exactly the same distance as in NiTe$_2$. The Ni–Te bond is extremely temperature-stable and well defined, as can be deduced from the values of the parameter σ^2_{Ni-Te}. The slight increase of disorder when going from 20 K to RT can be completely attributed to thermal vibrations, since the bond length remains almost constant with temperature. Second shell is divided into a Pb and a Ni sub-shell. At low temperatures, three to four Pb atoms are placed at the distance ≈ 3.71 Å, which is 0.15 Å shorter than in Ni–Ni distance in NiTe$_2$ (3.86 Å [19]) and only about 0.5 Å longer than the distance of the first coordination shell in PbTe:Ni (3.23 Å [20]). One to two Ni atoms are found at ≈ 3.85 Å, the distance
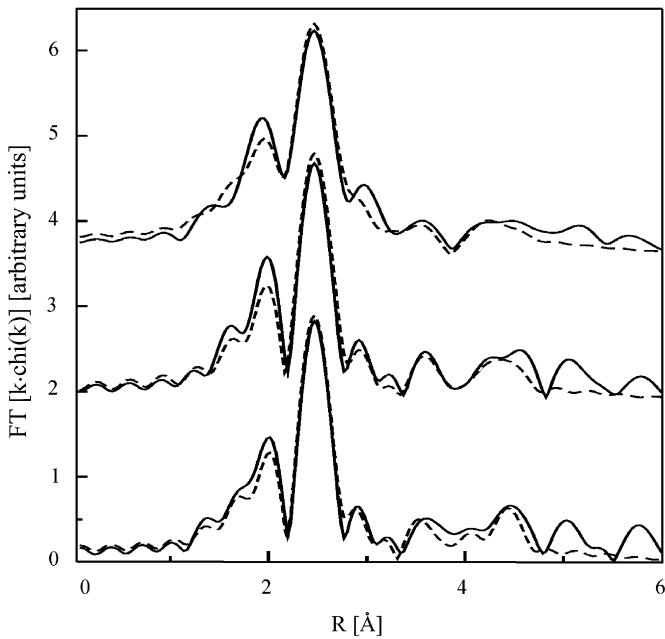
Fig. 2. Fourier transform of the k-weighted Ni K-edge EXAFS spectra taken at RT (upper part) 80 K (middle part) and 20 K (lower part). Full line represents experimental data, dashed line represents fit.

Table 1
Structural EXAFS parameters.

	20 K	80 K	295 K
E_0 (eV)	0.5(6)	0.7(7)	0.6(7)
R_{Ni-Te} (Å)	2.580(6)	2.582(6)	2.587(9)
σ^2_{Ni-Te}	0.0031(7)	0.0031(8)	0.007(1)
N_{Te}	5.3(4)	5.0(5)	5.3(4)
R_{Ni-Pb} (Å)	3.71(4)	3.70(5)	3.72(7)
σ^2_{Ni-Pb}	0.004(5)	0.005(8)	0.011(8)
N_{Pb}	3(1)	3(1)	4(1)
R_{Ni-Ni} (Å)	3.85(2)	3.85(3)	3.90(6)
N_{Ni}	3	3	2
R_{Ni-Te2} (Å)	4.51(2)	4.52(3)	4.58(7)
σ^2_{Ni-Te2}	0.006(3)	0.008(4)	0.02(1)

which is again the same as in NiTe$_2$. At RT both Ni–Pb and Ni–Ni bonds elongate and their disorder significantly increases. At low temperatures we were even able to locate Te atoms in the third coordination shell at distance which is slightly shorter than corresponding distance in NiTe$_2$ (4.55 Å [19]) and the distance of the second Pb shell in PbTe:Ni (4.56 Å [20]). Large thermal vibrations and probably also larger statistical disorder influence precise determination of the Ni–Te$_2$ distance at RT and the exact number of Te atoms in this shell (which was therefore fixed to expected six). These results could be indication of limited solubility of NiTe$_2$ in PbTe. However, according to our preliminary analysis of the EXAFS results obtained at Pb L$_{III}$-edge at 20 K, Pb sub-lattice is extremely stable and remains almost unaffected by the presence of Ni at this doping level. All the parameters up to the third shell, in consistency with XRD measurements [20], correspond to the NaCl-type structure. Despite the fact that there are no other crystalline phases in the sample, local structure around Ni atoms is to a large extent NiTe$_2$-alike as a result of stronger and predominately covalent Ni–Te bonding. Even though

long-range Coulomb interaction is expected to be strongly screened in PbTe compound due to the large dielectric constant, the Ni–Ni interaction is still strong enough to bring Ni atoms close to each other, even at this small concentration. Similar situation is observed in PbTe:Mn, only the transformation of the Mn immediate surrounding to MnTe was not completed which resulted in Mn off-centering from the regular PbTe lattice position [15,17]. Definite answers about Ni doping effects on PbTe will be possible to obtain after completing the Te K-edge data analysis.

In conclusion, we have studied nickel-doped PbTe by means of Ni K-absorption edge XAFS measurements at different temperatures. Detailed analysis of the XANES and EXAFS regions of the absorption spectra revealed that the local structure around Ni atoms strongly deviates from the host PbTe (NaCl) structure, and that it is very close to the CdI$_2$-type structure of NiTe$_2$ compound. Tellurium atoms in the immediate Ni surrounding form a temperature-stable octahedron whose orientation is adjusted to PbTe long-range order. The second, and even the third shell are also more NiTe$_2$ structure-alike. However, due to strong Coulomb screening and low Ni concentration, influence of Ni doping is localized and the long-range order is well preserved.

References

[1] M.S. Dresselhaus, G. Dresselhaus, X. Sun, Z. Zhang, S.B. Cronin, T. Koda, J.Y. Ying, Microscale Thermophysical Eng. 3 (1999) 89.
[2] J.H. Dughaish, Physica B 322 (2002) 205.
[3] K.F. Hsu, S. Loo, F. Guo, W. Chen, J.S. Dyck, C. Uher, T. Hogan, E.K. Polychroniadis, M.G. Kanatzidis, Science 303 (2004) 818.
[4] T.C. Harman, P.J. Taylor, M.P. Walsh, B.E. LaForge, Science 297 (2002) 2229.
[5] G. Grabecki, Mater. Sci.-Poland 24 (2006) 591.
[6] E. Kaufmann, G. Springholz, T. Schwarzl, G. Hesser, F. Schäffler, W. Heiss, K. Koike, T. Ikatura, T. Hotei, M. Yano, T. Wojtowicz, J. Phys.: Condens. Matter 20 (2008) 454216.
[7] Q.T. Islam, B.A. Bunker, Phys. Rev. Lett. 59 (1987) 2701.
[8] A.I. Lebedev, I.A. Sluchinskaya, Ferroelectrics 157 (1994) 275.
[9] D.T. Morelli, J.P. Heremans, C.M. Thrush, Phys. Rev. B 67 (2003) 035206.
[10] L.I. Rabova, D.R. Khokhlov, JETP Lett. 80 (2004) 133.
[11] A.I. Lebedev, I.A. Sluchinskaya, S.G. Nikitenko, S.G. Dorofeev, Phys. Scr. T 115 (2005) 365.
[12] S. Ahmad, S.D. Mahanti, K. Hoang, M.G. Kanatzidis, Phys. Rev. B 74 (2006) 155205.
[13] S. Ahmad, K. Hoang, S.D. Mahanti, Phys. Rev. Lett. 96 (2006) 056403.
[14] R. Saravanan, M. Charles Robert, J. Phys. Chem. Solids 70 (2009) 159.
[15] I. Radisavljević, N. Ivanović, N. Novaković, N. Romčević, H.-E. Mahnke, X-ray Spectrom. 36 (2007) 150.
[16] I. Radisavljević, N. Ivanović, N. Novaković, N. Romčević, H.-E. Mahnke, AIP Conf. Proc. 899 (2007) 642.
[17] I. Radisavljević, N. Ivanović, N. Novaković, M. Manasijević, N. Romčević, H.-E. Mahnke, M. Mitrić, J. Phys.: Condens. Matter, submitted.
[18] Y.P. Yadava, R.A. Singh, J. Mater. Sci. Lett. 4 (1985) 1421.
[19] F. Hulliger, Structural chemistry of layer type phases, in: F. Levy (Ed.), Physics and Chemistry of Materials with Layered Structures, Vol. 5, Reidel, Dordrecht, 1976.
[20] N. Romčević, J. Trajić, T.A. Kuznetsova, M. Romčević, B. Hadžić, D.R. Khokhlov, J. Alloys Compd. 442 (2007) 324.
[21] A.L. Ankudinov, C. Bouldin, J.J. Rehr, J. Sims, H. Hung, Phys. Rev. B 65 (2002) 104107.
[22] B. Ravel, J. Synchrotron Rad. 8 (2001) 314.
[23] M. Newville, J. Synchrotron Rad. 8 (2001) 322.
[24] B. Ravel, M. Newville, J. Synchrotron Rad. 12 (2005) 537.